Biogeosciences Discuss., 9, 557–579, 2012
www.biogeosciences-discuss.net/9/557/2012/
doi:10.5194/bgd-9-557-2012

Biogeosciences Discussions

Pyrite Oxidation under initially neutral pH conditions and in the presence of *Acidithiobacillus ferrooxidans* and micromolar hydrogen peroxide

Y. Ma[1] and C. Lin[2]

[1]Centre for Ecological and Environmental Technologies, South China Agricultural University, Guangzhou 510642 China
[2]Australian Centre for Sustainable Catchments, University of Southern Queensland, Toowoomba, QLD 4350 Australia

Received: 23 December 2011 – Accepted: 2 January 2012 – Published: 16 January 2012

Correspondence to: C. Lin (chuxia.lin@usq.edu.au)

Published by Copernicus Publications on behalf of the European Geosciences Union.

Abstract

Hydrogen peroxide (H_2O_2) at a micromolar level played a role in the microbial surface oxidation of pyrite crystals under initially neutral pH. When the mineral-bacteria system was cyclically exposed to 50 µM H_2O_2, the colonization of *Acidithiobacillus ferrooxidans* onto the mineral surface was markedly enhanced, as compared to the control (no added H_2O_2). This can be attributed to the effects of H_2O_2 on increasing the roughness of the mineral surfaces, as well as the acidity and Fe^{2+} concentration at the mineral-solution interfaces. All of these effects tended to create more favourable nano- to micro-scale environments in the mineral surfaces for the cell adsorption. However, higher H_2O_2 levels inhibited the attachment of cells onto the mineral surfaces, possibly due to the oxidative stress in the bacteria when they approached the mineral surfaces where high levels of free radicals are present as a result of Fenton-like reactions. The more aggressive nature of H_2O_2 as an oxidant caused marked surface flaking of the mineral surface. The XPS results suggest that H_2O_2 accelerated the oxidation of pyrite-S and consequently facilitated the overall corrosion cycle of pyrite surfaces. This was accompanied by pH drop in the solution in contact with the pyrite cubes.

1 Introduction

Oxidation of pyrite has been of great research interest for decades due to its significance in biomining (Rawlings and Johnson, 2007) and the formation of acid mine drainage and acid sulfate soils (Lin et al., 2008). The common oxidants causing the weathering of pyrite is molecular oxygen and ferric ion (Fe^{3+}); the latter is much stronger than the former in oxidizing pyrite (Moses et al., 1987). However, due to limited Fe^{3+} solubility, the aqueous Fe^{3+}-driven pyrite oxidation is generally inhibited under initially neutral pH conditions, such as that encountered in freshly exposed pyrite crystal surfaces. In such instances, molecular oxygen plays a more important role in pyrite oxidation, as compared to ferric ion.

Surface oxidation of pyrite by attached iron/sulfide-oxidizing bacteria is possible. Mielke et al. (Mielke et al., 2003) inoculated *Acidithiobacillus ferrooxidans* onto pyrite crystals and found that the bacteria were able to grow under circumneutral pH conditions. They suggested that the colonization of pyrite by the bacteria was facilitated by the development of an acidic nanoenvironment between the bacteria and the mineral surface where Fe^{3+}-driven pyrite oxidation took place.

Hydrogen peroxide (H_2O_2) is a much more aggressive oxidant than molecular oxygen (Rush et al., 1985; King, 1998). Unlike Fe^{3+}-driven pyrite oxidation, the H_2O_2-driven pyrite oxidation is not impeded at circumneutral pH. H_2O_2 is a common constitute of rainwater (Cooper et al., 1987; Willey et al., 1996; Yuan and Shiller, 2000). H_2O_2 can also be generated through radiolysis of water in geological formations or industrial wastes containing radioactive materials such as uranium ores, spent nuclear fuel etc. (Amme et al., 2005; Vovk, 1982). This implies that H_2O_2-pyrite contact scenarios are likely to occur in natural environments. Moreover, H_2O_2 has potential applications in hydrometallurgy for the extraction of base metals from sulfide ores (Antonijevic et al., 2004; Aydogan, 2006; Aydogan et al., 2007) and in desulfurization of coal (Ehsani, 2006). There is a possibility for the leaking/residual H_2O_2 to be in contact with pyrite in the non-target areas surrounding the heap leach piles.

Lefticariu et al. (2006, 2007) examined the effects of H_2O_2 on surface oxidation of pyrite under various temperature conditions. However, the concentration range of H_2O_2 (2–200 mM) that they used was far greater than that possibly encountered in natural environments. Furthermore, microbial factor was not considered in their study. It has been known that when H_2O_2 comes into contact with Fe^{2+}, the Fenton or Fenton-like chain reactions take place to generate hydroxyl radical (OH) and other free radicals, which are even more powerful than H_2O_2 in terms of oxidative capacity (Barbusinski, 2009). This could complicate the microbially mediated pyrite oxidation process through enhancing abiotic pyrite oxidation by reactive oxygen species (H_2O_2 and free radicals) on one hand and causing oxidative stress or damage in iron/sulfide-oxidizing bacteria on the other. The potentially integrative effect of H_2O_2 on the microbially mediated

pyrite oxidation has implication for better understanding the biogeochemical process related to the formation of acid mine drainage and acid sulfate soils.

There has been so far no work investigating microbially mediated oxidation of pyrite in the presence of H_2O_2. In this study, we examined the surface oxidation of single pyrite crystals at initial circumneutral pH and in the presence of an *Acidithiobacillus ferrooxidans* strain and H_2O_2. The objective was to determine whether H_2O_2 at micromolar levels has a role to play in microbially mediated pyrite weathering under initially neutral pH conditions.

2 Materials and methods

2.1 Pyrite specimens and pretreatment

The pyrite specimens used in this study were purchased from the Anfei Tongling Siling Mineral Ltd. Pyrite cubes with similar size (weight: 36 ± 4.9 g) were selected for the mineral-solution contact experiment. Prior to the experiment, the mineral crystals were treated with a boiling 6 M HCl solution to remove the oxidized materials possibly present on the original mineral surfaces. The "cleaned" pyrite cubes were immediately used for the experiment after washing with distilled water twice and acetone for three times.

2.2 Bacteria, culture conditions and inoculum preparation

A strain of *Acidithiobacillus ferrooxidans* was purchased from the Marine Culture Collection of China (MCCC). The bacterial culture were maintained at 4 °C in a 9 K nutrient medium containing 3.0 g of $(NH_4)_2SO_4$, 0.01 g of $Ca(NO_3)_2$, 0.5g of $MgSO_4.7H_2O$, 0.5g of K_2HPO_4, 0.1 g of KCl and 44.3 g of $FeSO_4.7H_2O$ in 1 l of distilled water with pH adjusted to 1.6 with a H_2SO_4 solution.

The inoculum was prepared prior to the experiment. An adequate amount of the bacteria required for the experiment was produced by facilitating bacterial growth in

a sterile 9 K medium at 30 °C, coupled with shaking (130 rpm) on a rotary shaker for 5–6 days. The cells in the enriched suspension were firstly separated from the iron precipitates (formed during the incubation) by centrifugation at 3000 rpm for 3 min to allow the settlement of the solid iron compounds. The cells remained in the suspension were then transferred into a new centrifuge tube and harvested by centrifugation at 5000 rpm for 10 min to allow the settlement of the cells. After washing twice with sterile distilled water (adjusted to pH 6.8 by a KOH solution), the inoculum was formed by adding an appropriate amount of the same distilled water into the centrifuge tube containing the cleaned cells. The cell concentration in the inoculum was determined by direct cell counting prior to addition into the experimental reactor. For this experiment, the cell concentration of the inoculum was 2.5×10^8 cells ml^{-1}.

2.3 Experimental design

A modified 9 K medium (without added $FeSO_4 7H_2O$) was used as the basal solution for the experiment. Pyrite cubes were exposed to various concentrations of H_2O_2 in the modified 9 K medium in the presence of the *Acidithiobacillus ferrooxidans* at an initial concentration of 2.5×10^7 cells ml^{-1}. One control (C, without added H_2O_2) and three treatments with different H_2O_2 concentrations were established: (a) Treatment 1 (T1): 50 µM; (b) Treatment 2 (T2): 100 µM; and (c) Treatment 3 (T3): 1000 µM.

A 100 ml centrifuge tube was used as the reaction chamber. In each tube, a pyrite cube was soaked with a relevant solution of the same mass (i.e. the mass ratio of solid to liquid was 1:1). The tube was loosely capped to allow entry of air but not dust during the entire period of the experiment except at the time of cyclic H_2O_2 injection, in-situ pH measurements and solution sample collection.

A time interval of 3–5 days was established for re-injection of H_2O_2. Because the volume of solution was less than 40 ml for each reactor, frequent sampling for determinations of chemical and biological parameters in the reacting solution was not appropriate. Therefore, solution sample collection was only undertaken at a few selected times.

After sampling, an equal amount of sterile 9 K medium was added into the reactor to compensate the solution loss caused by sample collection.

The reactors were placed in a biological incubator with temperature set at 30 °C during the entire period of experiment except during cyclic H_2O_2 injection and sample collection. The experiment was performed in five replicates and lasted for 108 days. At the end of the experiment, the pyrite cubes were harvested for surface characterization analysis both before and after treatment with a boiling 6 M HCl solution.

2.4 Analytical methods

In-situ measurement of pH in the solution was made by a calibrated pH meter. Ferrous ion (Fe^{2+}) in the reacting solutions was measured by the potassium perchromate titration method (Zhao et al., 2003). Total Fe was measured by an atomic absorption spectrometer. The planktonic cell concentration in the reacting solutions was determined by direct cell counting.

A FEI-XL30 environmental scanning electron microscope coupled with energy dispersive X-ray spectrometer (ESEM/EDS) was used for surface imaging of the pyrite cubes. The X-ray photoelectron spectroscopy (XPS) was employed to determine the chemical composition and element states of the reacted pyrite surfaces (prior to the boiling HCl treatment) and the corroded surface (after the boiling HCl treatment). XPS analyses were performed with a Kratos Axis Ultra^{DLD} spectrometer using a monochromatic Al Kα X-rays source. Broad scan was conducted using 160 eV pass energy, while narrow high-resolution spectra of all major lines were obtained using a resolution function with a width of 0.1 eV for a pass energy setting of 40 eV. The charge effect was corrected using C 1 s from contamination at 284.6 eV. Spectra were analyzed using the CasaXPS software (Version 2.2.19).

3 Experimental result analysis

3.1 Aqueous phase

There was a trend that the pH decreased with increasing incubation time for the control and all the three treatments with T3 (the highest dosage level of H_2O_2 in this study) having a marked drop in pH to 3.76 on the last day of the experiment (Fig. 1a). The total Fe measured from the bulk solution ranged from 0.16 to 0.55 mg l^{-1} for the 5 sampling occasions (details are provided in Table S1 in the Supplement). Since the method used for the measurement of aqueous Fe^{2+} had a detection limit of 1 mg l^{-1}, it was not possible to discriminate between Fe^{2+} fraction and Fe^{3+} fraction in the solution. However, because the pH of the bulk solutions was greater than 3.5, which limited the solubility of Fe^{3+}, it is more likely that Fe^{2+} dominated the total Fe in the solutions. Planktonic *Acidithiobacillus ferrooxidans* in the solutions were observed at least prior to the 51st day of the experiment. But there was a tendency that the cell population decreased over time (Fig. 1b).

3.2 SEM observations

Figure 2 shows the SEM images of the reacted pyrite cube surfaces for the control (C) and various treatments and the corroded surfaces for C and T1. There were cells attached to the mineral surfaces for C (no added H_2O_2) and T1 (50 µM H_2O_2 treatment) (Fig. 2a, b), while no attached cells were observed for T2 (100 µM H_2O_2 treatment) and T3 (1000 µM H_2O_2 treatment) (Fig. 2c, d). The microbial population density was much lower in C than in T1 (Fig. 2a, b). There was a marked difference between C and T1 in the distribution pattern of the corrosion pits in the mineral surfaces after the HCl treatment to remove the overlying oxidation products (Fig. 2e, f). The corrosion pits in C tended to be oriented along straight lines, which run parallel to each other (Fig. 2e and Fig. S1 in the Supplement). In contrast, T1 exhibited irregular distribution of corrosion pits (Fig. 2f). For T2 and T3, the characteristic pits of microbial corrosion were not

observed in the corroded mineral surfaces (Figs. S2 and S3 in the Supplement). For the treatments with the highest H_2O_2 dosage level (T3), extensive surface flaking was observed for the pyrite cubes before the boiling HCl treatment (Fig. 2d and Fig. S4 in the Supplement).

3.3 XPS analysis

The XPS results showed that within a ~3–5 nm thick surface layer, oxygen accounted for a large proportion (77–85 % on a molar basis) of the sum of iron, sulfur and oxygen. There was a trend that the oxygen percentage decreased with increasing dosage level of H_2O_2 in the solution (Fig. 3a). The Fe/S ratio of the reacted surfaces ranged from 0.82 to 1.28, which was much higher than the value (0.5) of the theoretical Fe/S ratio for pyrite; T3 (the highest dosage level of H_2O_2) had the lowest Fe/S ratio. After treatment of the pyrite cubes with the boiling HCl to remove the oxidized materials, the proportion of oxygen in the sum of iron, sulfur and oxygen markedly decreased for the outermost layer (top ~3–5 nm thick) of the corroded surface (Fig. 2b). In contrast with the reacted surface, the Fe/S ratio of the corroded surface ranged from 0.26 to 0.29, which was much lower than the theoretical Fe/S ratio for pyrite.

The XPS spectra for the reacted pyrite cube surfaces are shown in Fig. 4. For the control, T1 and T2, the Fe $2p_{3/2}$ spectra had two major peaks centred at 708.8 ± 0.20 eV and 712.6 ± 0.00 eV, respectively (Fig. 4a, Table 1, Figs. S5, S6 and S7 in the Supplement). The peak with the lower binding energy can be assigned to Fe^{2+} bonded to O^{2-} (Lefticariu et al., 2006, 2007) or Fe^{3+} bonded to S^- (Barbusinski, 2009) while the higher binding energy peak may be attributed to Fe^{3+} bonded to OH^-, O^{2-} or SO_4^{2-} (Lefticariu et al., 2007; Mills and Sullivan, 1983; Zhao et al., 2003). There was a trend that the proportion of (Fe^{2+})-(O^{2-})/(Fe^{3+})-(S^-) bond increased with increasing concentration of H_2O_2 in the solution while the opposite was observed for the (Fe^{3+})-(O^{2-})/(Fe^{3+})-(OH^-)/(Fe^{3+})-(SO_4^{2-}) bond. Although T3 also had two XPS Fe $2p_{3/2}$ peaks, both shifted to the lower binding energy side by 1.3 eV (centred at

707.5 eV) and 1.1 eV (centred at 711.5 eV), respectively (Fig. 4a, Table 1 and Fig. S8 in the Supplement). The 707.5 eV peak is characteristic of pyrite-Fe^{2+} (Barbusinski, 2009; Nesbitt et al., 1994, 1998). For S 2p XPS spectra, there were also two major peaks for the control, T1 and T2. The first peak was centred at 164.1 ± 0.20 eV and the second peak was centred at 165.3 ± 0.20 eV (Fig. 4b, Table 1, Figs. S9, S10 and S11 in the Supplement). S 2p XPS peak falling within the range of 163–165 eV was frequently attributed to polysulfides (S_n^{2-}) and their end product, elemental sulfur (S^o) (Barbusinski, 2009; Bonneissel-Gissinger et al., 1998; Cai et al., 2009; Ferris et al., 1989; Nesbitt et al., 1994, 1998). Similar to the Fe $2p_{3/2}$ spectrum, the two S 2p peaks for T3 shifted to the lower energy side by 1.3 eV (centred at 162.8 eV and 164.0 eV, respectively) (Fig. 4b, Table 1 and Fig. S12 in the Supplement). The 162.8 eV peak is typical of disulfide (S_2^{2-}) bonded to Fe^{2+} (Barbusinski, 2009; Bostick and Fendorf, 2003; Carlson, 1975; Nesbitt et al., 1998; Wagner et al., 1979).

After removal of the oxidation products on the mineral surfaces, the Fe 2p spectra for the corroded mineral surfaces showed a high degree of similarity among the control and the treatments (Fig 4c). There were two major peaks in the Fe $2p_{3/2}$ spectra; the lower binding energy one centred at 707.44 ± 0.03 eV and the higher binding energy one centred at 708.36 ± 0.23 eV (Fig. 4c, Table 1, Figs. S13, S14, S15 and S16 in the Supplement). The S 2p spectra also exhibited certain similarity among the control and the treatments, showing four major peaks centred at 162.78 ± 0.02, 163.95 ± 0.03, 164.41 ± 0.38, and 161.81 ± 0.01 (Fig. 4d, Table 1, Figs. S17, S18, S19 and S20 in the Supplement). The 161.81 eV peak can be attributed to monosulfide species (S^{2-}) bonded to Fe^{2+} (Lefticariu et al., 2007).

4 Discussion

4.1 Effects of H_2O_2 on the survival behavior of *Acidithiobacillus ferrooxidans*

There have been previous reports showing that surface microtopography of pyrite affects bacterial adhesion (Hyland and Bancroft, 1990). Bacteria may preferentially attach to scratch, pits and grooves on the surfaces of pyrite crystals (van der Heide et al., 1980). The pearl string-like chains of corrosion pits may reflect the strong control of bacterial corrosion by the crystal structure and on deviations in the crystal order (fracture lines and dislocations) of the leachable substrate (Mycroft et al., 1990). In contrast with the control, the corrosion pits in T1 exhibited irregular distribution and frequently appeared in clusters. These suggest that attachment of the cells onto the pyrite cube surfaces was not strictly limited to the originally favourable microtopographic or structural sites in the presence of H_2O_2 at a concentration of 50 µM. This explains the observed denser attached-cell population in T1 than in C. The extract mechanism responsible for the H_2O_2-facilitated colonization of *Acidithiobacillus ferrooxidans* on the pyrite crystal surfaces is not clear. Possibly, the more aggressive attack of H_2O_2 on the mineral surface assisted in creating favourable landing spots for the planktonic cells in otherwise non-microtopographically or non-structurally favourable locations. H_2O_2 has a much stronger capacity to oxidize pyrite, as compared to molecular oxygen. The initial attack of the pyrite surface by H_2O_2 was likely to increase the roughness of the mineral surfaces, as well as the acidity and Fe^{2+} concentration at the mineral-solution interfaces. All of these could boost the adsorption of planktonic cells onto the mineral surfaces and consequently promote the production of extracellular polymeric substance (EPS) at the microbe-mineral interface. The formation of biofilms provided shelters for the development of microbial colonies on the mineral surfaces and possibly created favourable micro-scale environment for catalysed pyrite oxidation at the cell-mineral interfaces. However, at higher concentration of H_2O_2, as encountered in T2 (100 µM) and T3 (1000 µM), the activities of *Acidithiobacillus ferrooxidans* might be

depressed due to oxidative damage or stress in the cells caused by the free radicals generated near the solution-mineral interfaces when H_2O_2 reacted with Fe^{2+} on the pyrite crystal surfaces. The production of Fenton reaction-derived hydroxyl radical can be described by the following chemical equation:

$$\text{Pyrite} - Fe^{2+} + H_2O_2 \longrightarrow \text{Pyrite} - Fe^{3+} + OH^{\bullet} + OH^{-} \quad (1)$$

The presence of toxic hydroxyl radical near the mineral surface was likely to prevent the planktonic cells from approaching the surface of pyrite cubes. This explains the absence of the attached cells and microbial corrosion pits in T2 and T3.

Although the colonization of *Acidithiobacillus ferrooxidans* in the mineral surface was inhibited at higher H_2O_2 concentrations in T2 and T3, the survival of planktonic cells in the solution was not threatened in these treatments at least before the 51st day of the experiment. This observation suggests that certain individual cells were able to adapt to high H_2O_2 conditions by developing H_2O_2 tolerance. It is not known whether the decrease in planktonic cell population over time reflected the adverse effects of H_2O_2–derived oxidative stress in the bacteria or was simply due to the insufficient supply of the solution-borne ferrous ion or reduced S species to support the growth of the bacteria. Further work is currently underway to obtain insights into the mechanisms.

4.2 Effects of H_2O_2 on the production of aqueous Fe and H^+

Since the planktonic *Acidithiobacillus ferrooxidans* only feed on aqueous Fe^{2+} or soluble reduced-S species such as thiosulfate or sulfite, the presence of planktonic cells suggests that the reacted mineral surface continued to release these chemical species into the solutions, which allowed the survival of the planktonic cells by providing them with essential foods. However, due to the small surface area of the single pyrite cubes used in the experiment, the amount of Fe^{2+} and soluble reduced-S species released from the mineral was likely to be limited. On the other hand, the aqueous Fe^{2+} was subject to rapid oxidation to Fe^{3+} and the subsequent hydrolysis to precipitate as insoluble iron compounds under the high pH conditions. The oxidation of aqueous Fe^{2+}

could also be enhanced in the presence of *Acidithiobacillus ferrooxidans*. These explain the observed low concentration of total Fe in the solutions. As mentioned above, the trend that the planktonic cell population decreased over time (Fig. 1b) might reflect the insufficient supply of aqueous Fe^{2+} and soluble reduced-S species to sustain the growth of *Acidithiobacillus ferrooxidans* under the experimental conditions. The decrease in pH over time can be attributed to the generation of H^+ as a result of aqueous Fe^{3+} hydrolysis in the solution. The marked pH drop in T3 was consistent with what is expected for the strong release of Fe from the mineral surface into the solution under the strongest H_2O_2 attack scenario set in this study.

4.3 Effects of H_2O_2 on the surface chemical states and their implications for understanding the chemical reactions at the solution-mineral interface

For the control, the Fe-deficient nature (as indicated by a much lower Fe/S ratio, relative to that of bulk pyrite) in the outermost layer (3 nm thick) of the corroded pyrite cubes suggests that pyrite-Fe was preferentially liberated from the pyrite cube surfaces during the incubation experiment. This can be explained by the relative easiness of the pyrite-Fe liberation reaction, as shown in the following overall chemical equation:

$$\text{Pyrite substrate} - [(S_2^{2-}) - (Fe^{2+})]^{o} - e^{-} \longrightarrow \text{Pyrite substrate} - S_2^{2-} + Fe^{3+}_{(aq)} \quad (2)$$

The completion of the above chemical reaction requires only one electron transfer from pyrite-Fe^{2+} to an electron acceptor (oxidant) in the solution. In contrast, the liberation of pyrite-S_2^{2-} requires multiple steps of electron transfer from the pyrite surface to electron acceptors. The minimum number of electrons needed to be transferred to the external oxidants in order to liberate one pyrite-S atom is 3 according to the equation below:

$$\text{Pyrite substrate} - [(Fe^{2+}) - (S_2^{2-})]^{o} - 3e^{-} \longrightarrow \text{Pyrite substrate} - [(Fe^{2+}) - (S^{-})]^{+} + S^{2+}$$
$$(\text{as in } S_2O^{2-}_{3(aq)}) \quad (3)$$

The complete release of 2 pyrite-S atoms in one pyrite molecule therefore requires 6 electrons being transferred from the pyrite surface to the external electron acceptors, as shown below:

$$\text{Pyrite substrate} - [(Fe^{2+}) - (S_2^{2-})]^{o} - 6e^{-} \longrightarrow Fe^{2+}_{(aq)} + 2S^{2+}(\text{as in } S_2O^{2-}_{3(aq)}) \quad (4)$$

It is therefore understandable that oxidation of pyrite-S_2^{2-} did not keep pace with the oxidation of pyrite-Fe^{2+}, leaving sulfur species of intermediate oxidation states remained structurally connected with the pyrite substrate. This can be illustrated by the following possible chemical reactions:

$$\text{Pyrite substrate} - [(S_2^{2-}) - (Fe^{2+})]^{o} - e^{-} \longrightarrow \text{Pyrite substrate} - [(S_2^{2-}) - (Fe^{3+})]^{+} \quad (5)$$

$$\text{Pyrite substrate} - [(S_2^{2-}) - (Fe^{3+})]^{+} - e^{-} \longrightarrow \text{Pyrite substrate} - [(S_2^{-}) - (Fe^{3+})]^{2+} \quad (6)$$

$$\text{Pyrite substrate} - [(S_2^{-}) - (Fe^{3+})]^{2+} \longrightarrow \text{Pyrite substrate} - 2S^{o} + Fe^{2+}_{(aq)} \quad (7)$$

$$\text{Pyrite substrate} - 2S^{o} - 2e^{-} \longrightarrow \text{Pyrite substrate} - S^{o} + S^{2+}(\text{as in } S_2O_3^{2-}) \quad (8)$$

$$\text{Pyrite substrate} - S^{o} - 2e^{-} \longrightarrow \text{Pyrite substrate} - [(S_2^{2-}) - (Fe^{2+})]^{o}(\text{next layer}) + S^{2+} (\text{as in } S_2O_3^{2-}) \quad (9)$$

$$Fe^{2+}_{(aq)} - e^{-} \longrightarrow Fe^{3+}_{(aq)} \quad (10)$$

$$Fe^{3+}_{(aq)} + 2H_2O \longrightarrow FeOOH_{(s)} + 3H^{+} \quad (11)$$

$$Fe^{2+}_{(aq)} + 2Fe^{3+}_{(aq)} + 4H_2O \longrightarrow Fe_3O_{4(s)} + 8H^{+} \quad (12)$$

$$S_2O^{2-}_{3(aq)} - 8e^{-} \longrightarrow 2SO^{2-}_{4(aq)} \quad (13)$$

$$3Fe^{3+}_{(aq)} + 6H_2O + 2SO^{2-}_{4(aq)} + K^{+}_{(aq)} \longrightarrow KFe_3(OH)_6(SO_4)_{2(s)} + 6H^{+} \quad (14)$$

Equation (5) represents the first step of cathodic reaction for a surface pyrite oxidation cycle. With the increase in the number of electrons being transferred from the mineral surface to the external oxidants, surface surfur evolved from disulfide (Eq. 5) to polysulfides (Eq. 6) to elemental sulfur (Eqs. 7 and 8). The old cycle ends at and the new cycle starts from Eq. (9). In reality, reaction products for the above reactions may co-exist in the outermost layer of the mineral surface. Equation (6) should be understood to represent a series of chemical reactions yielding various polysulfide species of different valences with a general formula of $S_n^{(n-m)-}$ ($n > 2$; $n > m > 1$). After pyrite-Fe is liberated from the mineral surface (Eq. 7), the availability of solution-borne oxidants (electron acceptors) should control the dominant sulfur species on the mineral surface according to Eqs. (8) and (9). The shift of the XPS S2p peaks (the reacted pyrite cube surfaces) to the lower binding energy side from C to T1 to T2 to T3 indicates a decrease in the average oxidation state of surface sulfur species with increasing dosage level of H_2O_2. This implies that an increase in the H_2O_2 strength enhanced the removal of intermediary sulfur species from the mineral surface, resulting in sulfur species with lower oxidation states occurring in the outermost 3 nm-thick surface layer or even exposed at the mineral surfaces. The appearance of surface (Fe^{2+})-(S_2^{2-}) bond in T3 reflects that part of the reacted surface was in a chemical state, as described in Eq. (9). The above data interpretation allows a conclusion to be drawn that the presence of H_2O_2 may accelerate the oxidation of pyrite-S and consequently facilitate the overall surface oxidation cycle of pyrite.

The dominant presence of oxygen, combined with the higher Fe/S ratio in the reacted pyrite cube surface (relative to that of bulk pyrite) suggests that iron oxide/oxyhydroxide coatings (Eqs. 11 and 12) had a thickness of at least 3 nm. The lack of sulfur species of higher valence states indicates that basic sulfate minerals such as jarosite (Eq. 14) were not precipitated on the pyrite cube surfaces. However, this does not necessarily mean that no sulfur oxyanion species were generated from the pyrite oxidation. As

shown in Eqs. (3), (8) and (9), thiosulfate could be formed during the surface oxidation of pyrite and went further oxidation to form sulfate (Eq. 13) in the solution. However, the formation of basic sulfate minerals might be impeded because the pH was too high to favour the process. Therefore, any sulfur oxyanions formed were primarily released into the solution.

5 Conclusions

The presence of an appropriate level of H_2O_2 markedly facilitated the colonization of *Acidithiobacillus ferrooxidans* onto the surfaces of pyrite cube due to the effects of H_2O_2 on creating more favourable nano- to micro-scale environments in the mineral surfaces for the cell adsorption. However, higher H_2O_2 levels inhibited the attachment of cells onto the mineral surfaces, possibly due to the oxidative stress in the bacteria when they approached the mineral surfaces where high levels of free radicals are present as a result of Fenton-like reactions. The planktonic *Acidithiobacillus ferrooxidans* were able to survive under the highest H_2O_2 dosage (1000 µM) conditions, possibly because of the relatively weak oxidative stress while swimming in the solution with a lower level of free radicals, as compared to the mineral-solution interfaces. However, the population of planktonic cells tended to decrease over time due to insufficient supply of aqueous Fe^{2+} and soluble reduced-S species to sustain the growth of *Acidithiobacillus ferrooxidans* under the experimental conditions. The more aggressive nature of H_2O_2 as an oxidant caused marked surface flaking of the mineral surface. The presence of H_2O_2 accelerated the oxidation of pyrite-S and consequently facilitated the overall corrosion cycle of pyrite surfaces. This caused the generation of H^+ and therefore the pH drop in the solution as a result of aqueous Fe^{3+} hydrolysis.

Supplementary material related to this article is available online at: http://www.biogeosciences-discuss.net/9/557/2012/bgd-9-557-2012-supplement.pdf.

Acknowledgements. This work was financially supported by the Natural Science Foundation of China (Project numbers: 40471067 and 40773058) and the Guangdong Bureau of Science and Technology (Project No. 2005A30402006).

References

Amme, M., Bors, W., Michel, C., Stettmaier, K., Rasmussen, G., and Betti, M.: Effects of Fe(II) and hydrogen peroxide interaction upon dissolving UO_2 under geologic repository conditions, Environ. Sci. Technol., 39, 221–229, 2005.

Antonijevic, M. M., Jankovic, Z. D., and Dimitrijevic, M. D.: Kinetics of chalcopyrite dissolution by hydrogen peroxide in sulphuric acid, Hydrometallurgy, 71, 329–334, 2004.

Aydogan, S.: Dissolution kinetics of sphalerite with hydrogen peroxide in sulphuric acid medium, Chem. Eng. J., 123, 65–70, 2006.

Aydogan, S., Erdemoglu, M., Ucar, G., and Aras, A.: Kinetics of galena dissolution in nitric acid solutions with hydrogen peroxide, Hydrometallurgy, 88, 52–57,, 2007.

Barbusinski, K.: Fenton reaction – Controversy concerning the chemistry, Eco. Chem. Eng., 16, 347–357, 2009.

Bonneissel-Gissinger, P., Alnot, M., Ehrhardt, J. J., and Behra, P.: Surface oxidation of pyrite as a function of pH, Environ. Sci. Technol., 32, 2839–2845, 1998.

Bostick, B. C. and Fendorf, S.: Arsenite sorption on troilite (FeS) and pyrite (FeS_2), Geochim. Cosmochim. Ac., 67, 909–921, 2003.

Cai, Y., Pan, Y., Xue, J., Sun, Q., Su, G., and Li, X.: Comparative XPS study between experimentally and naturally weathered pyrites, Appl. Surf. Sci., 255, 8750–8760, 2009.

Carlson, T. A.: Photoelectron and Auger Spectroscopy, Plenum Press, New York, 1975.

Cooper, W. J., Saltzman, E. S., and Zika, R. G.: The contribution of rainwater to variability in surface ocean hydrogen peroxide, J. Geophys. Res., 92, 2970–2980, 1987.

Ehsani, M. R.: Desulfurization of Tabas Coals Using Chemical Reagents, Iran. J. Chem. Chem. Eng., 25, 59–66, 2006.
Ferris, F. G., Tazaki, K., and Fyfe, W. S.: Iron oxides in acid mine drainage environments and their association with bacteria, Chem. Geol., 74, 321–330, 1989.
Hyland, M. M. and Bancroft, G. M.: Palladium sorption and reduction on sulphide mineral surfaces: An XPS and AES study, Geochim. Cosmochim. Ac., 54, 117–130, 1990.
King, D. W.: Role of carbonate speciation on the oxidation rate of Fe(II) in aquatic systems, Environ. Sci. Technol., 32, 2997–3003, 1998.
Lefticariu, L., Pratt, L. M., and Ripley, E. M.: Mineralogic and sulfur isotopic effects accompanying oxidation of pyrite in millimolar solutions of hydrogen peroxide at temperatures from 4 to 150 °C, Geochim. Cosmochim. Ac., 70, 4889–4905, 2006.
Lefticariu, L., Arndt, S. A., and Pratt, L. M.: Oxygen isotope partitioning during oxidation of pyrite by H_2O_2 and its dependence on temperature, Geochim. Cosmochim. Ac., 71, 5072–5088, 2007.
Lin, C., Huang, S., and Li, Y.: Proceedings of the Joint Conference of the 6th International Acid Sulfate Soil Conference and the Acid Rock Drainage Symposium, Guangdong Science and Technology Press, Guangzhou, 2008.
Mielke, R. E., Pace, D. L., Porter, T., and Southam, G.: A critical stage in the formation of acid mine drainage: Colonization of pyrite by Acidithiobacillus ferrooxidans under pH-neutral conditions, Geobiology, 1, 81–90, 2003.
Mills, P. and Sullivan, J. L.: A study of the core level electrons in iron and its three oxides by means of X-ray photoelectron spectroscopy, J. Phys. D: Appl. Phys., 16, 723–732, 1983.
Moses, C. O., Nordstrom, D. K., Herman, J. S., and Mills, A. L.: Aqueous pyrite oxidation by dissolved oxygen and by ferric iron, Geochim. Cosmochim. Ac., 51, 1561–1571, 1987.
Mycroft, J. R., Bancroft, G. M., McIntyre, N. S., Lorimer, J. W., and Hill, I. R.: Detection of sulphur and polysulphides on electrochemically oxidized pyrite surfaces by X-ray photoelectron spectroscopy and Raman spectroscopy, J. Electroanal. Chem., 292, 139–152, 1990.
Nesbitt, H. W. and Muir, I. J.: X-ray photoelectron spectroscopic study of a pristine pyrite surface reacted with water vapour and air, Geochim. Cosmochim. Ac., 58, 4467–4679, 1994.
Nesbitt, H. W., Bancroft, G. M., Pratt, A. R., and Scaini M. J.: Sulfur and iron surface states on fractured pyrite surfaces, Am. Mineral., 83, 1067–1076, 1998.
Rawlings, D. E. and Johnson, D. B.: The microbiology of biomining: Development and optimization of mineral-oxidizing microbial consortia, Microbiology, 153, 315–324, 2007.

Rush, J. D. and Bielski, B. H. J.: Pulse radiolytic studies of the reactions of HO_2/O_2^- with Fe(II)/Fe(III) ions, The reactivity of HO_2/O_2^- with ferric ions and its implication on the occurrence of the Haber–Weiss reaction, J. Phys. Chem., 89, 5062–5066, 1985.
van der Heide, H., Hemmel, R., van Bruggen, C. F., and Haas, C.: X-ray photoelectron spectra of 3d transition metal pyrites, J. Solid State Chem., 33, 17–25, 1980.
Vovk, I. F.: Radiolysis of underground waters as the mechanism of geochemical transformation of the energy of radioactive decay in sedimentary rocks, Lithol. Miner. Resour., 16, 328–334, 1982.
Wagner, C. D., Riggs, W. M., Davis, L. E., Moulder, J., and Muilenberg, G. E.: Handbook of X-ray photoelectron spectroscopy, Physical Electronics, Eden Prairie, Minnesota, 1979.
Willey, J. D., Kieber, R. J., and Lancaster, R. D.: Coastal rainwater hydrogen peroxide: Concentration and deposition, J. Atmos. Chem., 25, 149–165, 1996.
Yuan, J. and Shiller, A. M.: The variation of hydrogen peroxide in rainwater over the South and Central Atlantic Ocean, Atmos. Environ., 34, 3973–3980, 2000.
Zhou, J., Niu, Y., and Qin, W.: Effects of sulfide minerals on acidithiobacillus ferrooxidans, Chin. J. Nonferr. Metal., 13, 1278–1282, 2003.

Table 1. Binding energy (BE) and percent area of the major XPS Fe $2p_{3/2}$ and S 2p peaks of the reacted surface (before HCl treatment) and the corroded surface (after HCl treatment) for the control and various H_2O_2 treatments.

Treatment	BE (eV)	Peak area (%)
Fe 2p3/2 (Reacted surface)		
C	709.0	17
	712.6	83
T1	708.9	20
	712.6	80
T2	708.6	23
	712.6	77
T3	707.5	28
	711.5	72
S 2p (Reacted surface)		
C	164.3	70
	165.5	30
T1	164.1	68
	165.2	32
T2	163.9	67
	165.1	33
T3	162.8	67
	164.0	33
Fe 2p3/2 (Corroded surface)		
C	707.5	66
	708.3	34
T1	707.4	63
	708.4	37
T2	707.4	69
	708.1	31
T3	707.5	65
	708.1	35
S 2p (Corroded surface)		
C	162.8	55
	163.9	22
	164.0	21
	161.8	2
T1	162.8	61
	163.9	31
	164.9	6
	161.8	3
T2	162.8	62
	163.9	28
	164.6	7
	161.8	3
T3	162.8	60
	163.9	25
	164.4	12
	161.9	3

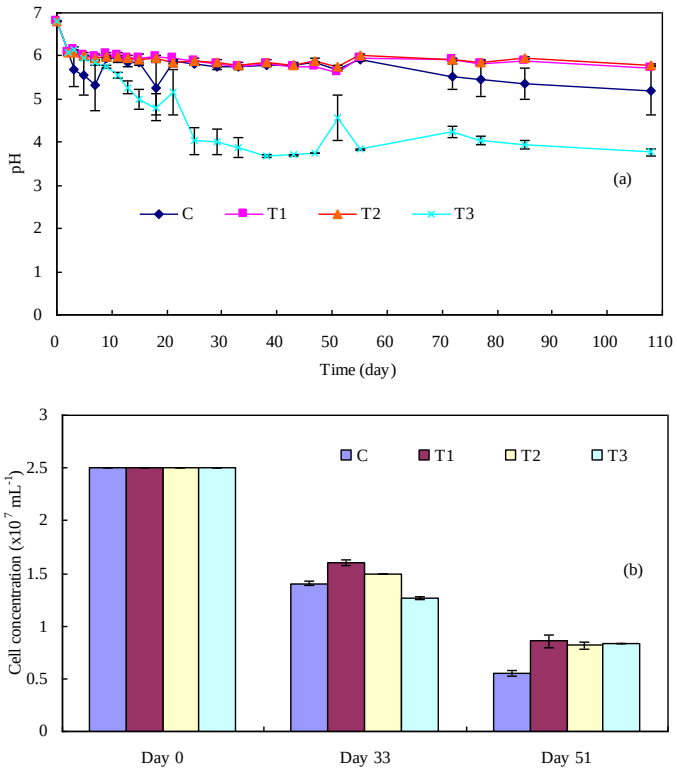

Fig. 1. Changes in **(a)** pH and **(b)** population of planktonic cells in the reacting solution during the period of the incubation experiment.

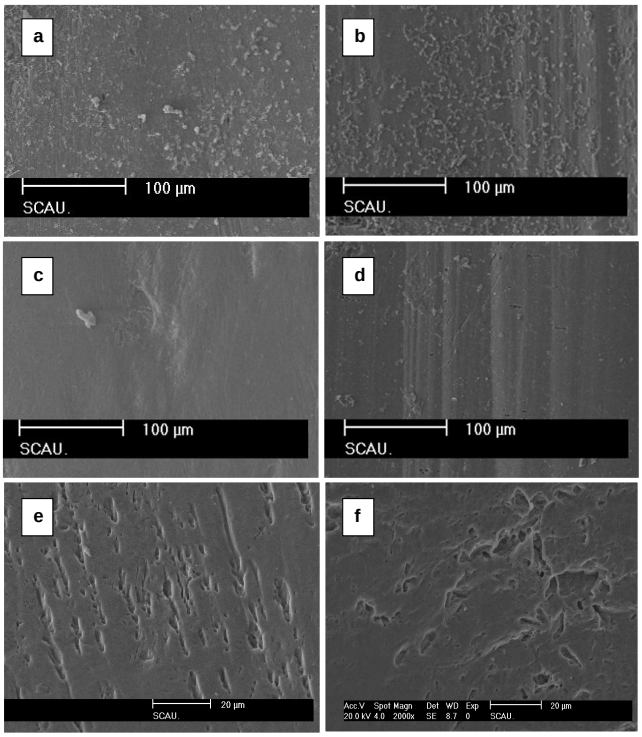

Fig. 2. SEM images showing **(a–d)** the reacted surface of pyrite cubes for the control (C), 50 µM H_2O_2 treatment (T1), 100 µM H_2O_2 treatment (T2), and 1000 µM H_2O_2 treatment (T3), respectively and **(e)** and **(f)** the corroded surface of the pyrite cubes for the control and T1.

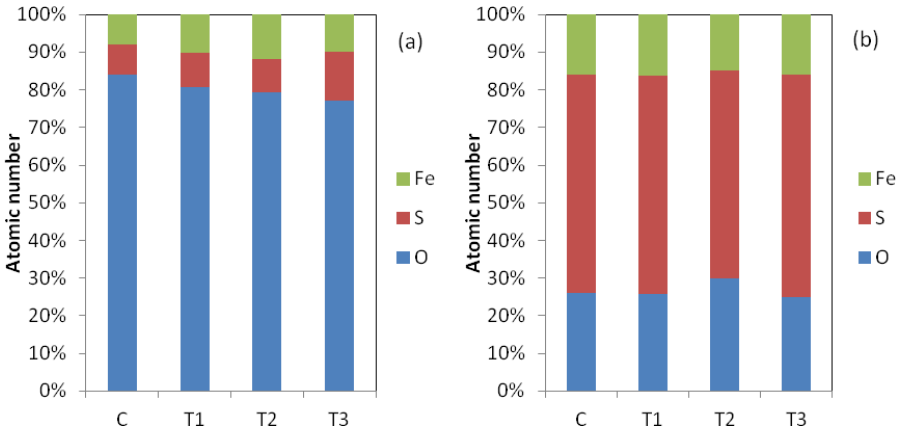

Fig. 3. Comparison of chemical composition (normalized to oxygen, sulfur and iron) in **(a)** the reacted pyrite cube surface and **(b)** the corroded pyrite cube surface among the control and the three treatments.

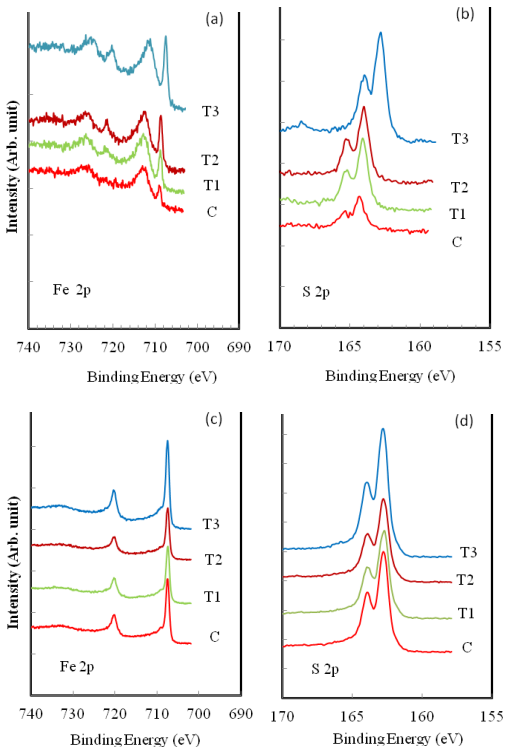

Fig. 4. Comparison of XPS spectra among the control and the three treatments. **(a)** XPS Fe $2p_{3/2}$ spectra of the reacted pyrite cube surfaces, **(b)** XPS 2p spectra of the reacted pyrite cube surfaces, **(c)** XPS Fe $2p_{3/2}$ spectra of the corroded pyrite cube surfaces, and **(d)** XPS 2p spectra of the corroded pyrite cube surfaces.